Indian Journal of Pure & Applied Physics
Vol. 62, October 2024, pp. 897-910
DOI: 10.56042/ijpap.v62i10.11811

Optimizing the Corrosion Parameters and Assessing Corrosion Inhibitions for Cast $Cu_{45}Mn_{25}Al_{15}Fe_5Cr_5Ni_5$ HEA in Nitric Acid Solution via DOE and RSM Analysis

Ghalia A Gaber[a], Hayam A Aly[b,c], Khaled A Abdelghafar[c] & Lamiaa Z Mohamed[d*]

[a]Department of Chemistry, Faculty of Science (Girls), Al-Azhar University, P.O. Box: 11754, Yousef Abbas St., Nasr City, Cairo, Egypt

[b]Department of Metallurgical and Materials Engineering, Faculty of Petroleum and Mining Engineering, Suez University, P.O. Box 43721, Suez, Egypt

[c]Metal casting lab, Central Metallurgical Research and Development Institute (CMRDI), P.O. Box 11421, Helwan, Egypt

[d]Mining, Petroleum and Metallurgical Engineering Department, Faculty of Engineering, Cairo University, Egypt

Received 13 June 2024; accepted 4 September 2024

The corrosion performance of the cast $Cu_{45}Mn_{25}Al_{15}Fe_5Cr_5Ni_5$ HEA was examined in HNO_3 solutions of varying concentrations (0.5%, 1%, 5%, and 10%). The microstructure and elemental composition of the alloy were examined using scanning electron microscopy (SEM) and energy dispersive X-ray analysis (EDX). Corrosion behavior was assessed through the weight-loss method at room temperature. To gain a thorough understanding of the corrosion parameters, both statistical analysis and interaction plots were utilized. Central composite design (CCD) was applied to investigate the primary and interaction effects of these parameters on the response. The optimal parameters for maximizing output were determined. Response Surface Methodology (RSM) with conditions of 24 h, 5% HNO_3 concentration, and a pH of 0.248 predicted a maximum fit of 81.64%. RSM also allows for more detailed analyses of the individual and interaction effects between the variables. The corrosion rate (CR) increased with higher HNO_3 concentrations. When 0.5% $HNO_3$was used, the inhibitor additions of Nano-TiO_2, Nan-SiO_2, or Nano-ZnO resulted in decreased CR values from 1.04 mm/y to 0.11, 0.12, or 0.22 mm/y, respectively.

Keywords: $Cu_{45}Mn_{25}Al_{15}Fe_5Cr_5Ni_5$ HEA; Corrosion inhibition; Corrosive media; Microstructure; Experimental correlations

1 Introduction

Globally, corrosion of metals and alloys is a problem in both natural and industrial settings. The corrosion negatively impacts industrial equipment, infrastructure asset life spans, and environmental quality. Therefore, to avoid monetary losses associated with materials, equipment, and structures, it is essential to develop and apply corrosion protection methods[1-3]. Copper alloys, renowned for their versatile chemical properties, find significant applications in environments containing HNO_3. These alloys exhibit notable resistance to corrosion by HNO_3, owing to their inherent chemical stability and protective oxide layers. Cu-alloys are very important for making sure that processes using HNO_3 are safe and effective in fields like chemical manufacturing, metallurgy, and pharmaceuticals[4,5]. This is because they are very resistant to chemicals and last a long time.

High-entropy alloys (HEAs) are a new type of material that can be told apart from other materials because of how they are made. They usually have equal or nearly equal amounts of several main elements[6,7]. These alloys exhibit remarkable mechanical, physical, and chemical properties, distinguishing them from conventional alloys[8]. Cu-based high entropy alloys (Cu-HEAs) are a notable subset of HEAs, leveraging copper as a primary constituent alongside other elements such as nickel, aluminum, and manganese. Cu-HEAs offer a wide range of tunable properties, including high strength, ductility, and corrosion resistance, making them highly desirable for applications in diverse fields such as aerospace, automotive, and electronics. These alloys have demonstrated exceptional performance in challenging environments, including high temperatures and corrosive atmospheres, showcasing their potential for next-generation materials engineering. With ongoing research and development efforts focused on optimizing their microstructure and

*Corresponding author: (E-mail: lamiaa.zaky@cu.edu.eg)

properties, Cu-HEAs hold great promise for addressing critical engineering challenges and advancing innovation in various industries[9,10].

Laboratory design, research, and product or formula development utilize the Design of Experiment (DOE), a statistical approach. Various industries widely utilize it to identify the optimal parameters from numerous variables or factors, thereby enhancing process yield, reducing variability, and lowering overall costs. DOE serves as a robust quantitative analysis tool in experimental design, employing techniques such as Central Composite Design (CCD), Response Surface Methodology (RSM), full factorial analysis, and Taguchi design, among others[11]. The RSM is an experimental model that primarily aims to approximate a complex, unknown function using a low-order polynomial[12]. To optimize the response or output, this method integrates mathematical and statistical techniques to model and analyze problems where multiple variables affect the response. It is particularly well-suited for optimization processes, as it can predict the optimal parameters, save time, and reduce experimental costs[13].

Chemical inhibitors are substances introduced into a corrosive environment to reduce or prevent the corrosion of materials exposed to that environment[14]. These inhibitors work by altering the chemical properties of the environment or forming a protective layer on the material's surface, thereby inhibiting corrosion reactions. Chemical inhibitors can be organic or inorganic compounds and are selected based on factors such as the type of corrosive environment, the material being protected, and the desired level of corrosion inhibition. Common types of chemical inhibitors include corrosion inhibitors, which protect metals from corrosion in aqueous environments, and scale inhibitors, which prevent the formation of scale deposits in industrial systems. Inhibitors stop corrosion and protect metals by making the anodic or cathodic polarizationbehavior (Tafel curves) better, stopping the transport or diffusion of ions to the metal surface, or increasing the electrical resistance of the metal surface[15].

TiO_2 has gained considerable attention because of its biological and chemical stability, affordability, ease of production, and environmentally friendly properties[16]. The ZnO nanoparticles, resembling white powder and insoluble in water, demonstrate outstanding electrical, chemical, and thermal stability. Their energy band of 3.37 eV and bonding energy of 60 meV are responsible for this. Additionally, they are safe, cost-effective, and simple to prepare[17,18]. Various corrosive environments, including HNO_3 solutions, commonly use TiO_2, SiO_2, and ZnO as chemical inhibitors. These metal oxides operate by creating protective layers on the surface of metal substrates, effectively inhibiting corrosion. TiO_2, SiO_2, and ZnO nanoparticles possess unique properties that contribute to their inhibitive performance. They have high surface areas, which promote their adsorption onto metal surfaces, forming dense and adherent protective films. These films act as barriers, preventing the penetration of corrosive agents and inhibiting the initiation and propagation of corrosion reactions. Additionally, TiO_2, SiO_2, and ZnO exhibit inherent chemical stability and resistance to acid attack, ensuring long-lasting corrosion protection. Because they are good at stopping corrosion in HNO_3 environments, they are useful as additives in many industrial settings, where metal equipment and infrastructure needs to stay strong and last a long time[19].

This study aimed to investigate the corrosion characteristics of cast $Cu_{45}Mn_{25}Al_{15}Fe_5Cr_5Ni_5$ HEA across various concentrations of HNO_3. The statistical analysis software MINITAB 18 was employed to design and analyze experiments, quantifying the effects of different parameters on the corrosion behavior of the HEA. Additionally, the impact of inhibitors such as Nan-TiO_2, Nano-SiO_2, and Nano-ZnO on corrosion behavior in a 0.5% HNO_3 solution was evaluated. Microstructural analysis and elemental composition assessments were performed both before and after exposure to HNO_3, providing a comprehensive understanding of the alloy's response to corrosive environments.

2 Experimental work

2.1 Material

An alloy with the nominal composition $Cu_{45}Mn_{25}Al_{15}Fe_5Cr_5Ni_5$ HEA was fabricated through the casting process using high-purity elements (99.9% pure) of Cu, Ni, Al, Cr, Mn, and Fe as raw materials. The alloy was manufactured by arc-melting the charge under vacuum conditions, followed by triple re-melting to guarantee uniformity. Samples were then obtained from the cast ingot using a wire-cutting machine. A Niton XL3T XRF portable analyzer was used to determine the ingot's chemical makeup. As a next step, samples were prepared for various types of

microscopies, including optical microscopy, scanning electron microscopy (SEM), and energy dispersive X-ray diffraction (EDX). Table 1 outlines the chemical composition of the cast ingot.

2.2 Corrosion Studies

The corrosion behavior of the cast $Cu_{45}Mn_{25}Al_{15}Fe_5Cr_5Ni_5$ HEA was assessed through chemical immersion tests to investigate the influence of Ni, Fe, and Cr additions. In glass vessels, 20 ml of 0.5%, 1%, 5%, and 10% HNO_3 solutions were utilized to determine the weight loss (WL) of the$Cu_{45}Mn_{25}Al_{15}Fe_5Cr_5Ni_5$ HEA. Adding 0.4 g of Nano-TiO_2, Nano-SiO_2, or Nano-ZnO all with 99.9% purity, were used as inhibitors. The samples underwent immersion for 120 h at a temperature of 20 ± 1 °C. Before immersion, the HEA surfaces were polished using 1000-grit emery paper, degreased with acetone, rinsed with doubly distilled water, dried, and then weighed on an analytical scale. Subsequently, the weighed coupons were placed in 20 mL of HNO_3 solutions with varying concentrations. After immersion, the $Cu_{45}Mn_{25}Al_{15}Fe_5Cr_5Ni_5$ HEA samples were taken out, rinsed with distilled water and acetone, dried, and reweighed. This experimental process was repeated multiple times, and the average WL values were recorded. Following this, the average corrosion rate (CR) values were calculated[20-22].

$$\mathrm{CR\ (mm/y)} = \frac{\Delta W \times K}{A \times T \times D} \quad \ldots (1)$$

K represents a constant (8.76×10^4), T presents the time in h, A is the section area in cm², ΔW is the loss of sample weight in grams, and D presents the density in g/cm³.

Theefficiency (I.E.) percentage and surface coverage (θ) are found in Eqs. 2 and 3[22,23]:

$$\%IE = (CR_0 - CR_{inh} / CR_0) \times 100 \quad \ldots(2)$$

CR_0 and CR_{inh} are the C.R. values of CADI with/without SBIs, respectively.

$$\theta = IE/100 \quad \ldots(3)$$

2.3 Surface Morphology

The specimens' surface morphologies, along with spot EDX analysis and elemental distribution mapping, were meticulously scrutinized within both 5% and 10% HNO_3 solutions.

Table 1 — Chemical composition of cast $Cu_{45}Mn_{25}Al_{15}Fe_5Cr_5Ni_5$ HEA in at. %

Element (%at.)	Cu	Mn	Al	Ni	Fe	Cr
Nominal composition	45	25	15	5	5	5
Actual composition	44.02	26.01	12.89	6.19	5.58	5.31

2.4 DOE and ANOVA

The DOE employs RSM with CCD to identify the variables that correlate throughout the trial[23]. Identifying the optimal course of action among multiple process variables is a common application of CCD[24]. Table 2 shows the selected three parameters and their corresponding levels. The next phase involves designing the experimental runs. All factors have high (+1) and low (-1) levels established based on historical data. Table 2 contains detailed information regarding the components and their respective levels.

To configure all the settings and values, it can utilize the software MINITAB. Automatic adjustments were applied to the parametric values, and the DOE model with the specified number of runs was established. Twenty runs are necessary for the developed model, with some duplication in the middle of the trial run combination. Using statistical tools, the experimental model is randomly generated based on the components and levels, producing the experimental worksheet. Fig. 1 displays a screenshot of Minitab, which generates the random worksheet. This random worksheet helps minimize experimental bias while Fig. 2 illustrates the results of the trial runs.

To evaluate the significance of each variable and their interactions, Analysis of Variance (ANOVA) is utilized. ANOVA is utilized to determine how categorical independent factors influence an interval-dependent variable and to identify key interactions among them[25]. The F-tests within ANOVA are crucial for analyzing experimental designs and identifying major effects and interactions.

3 Results and Discussion

3.1 Cast $Cu_{45}Mn_{25}Al_{15}Fe_5Cr_5Ni_5$ HEA

Figure 3 illustrates the microstructure of the cast $Cu_{45}Mn_{25}Al_{15}Fe_5Cr_5Ni_5$ HEA, showing the formation of two distinct phases. The matrix consists of a copper-rich phase, while the dispersed phase is also copper-rich. According to the EDX analysis, the

Table 2 — Design of experiment factors

			Level	
No.	*Factors*	*Notation*	*Low*	*High*
			-1	+1
1	Time, h	A	24	120
2	Conc., %	B	0.5	10.0
3	pH	C	0.114	0.360

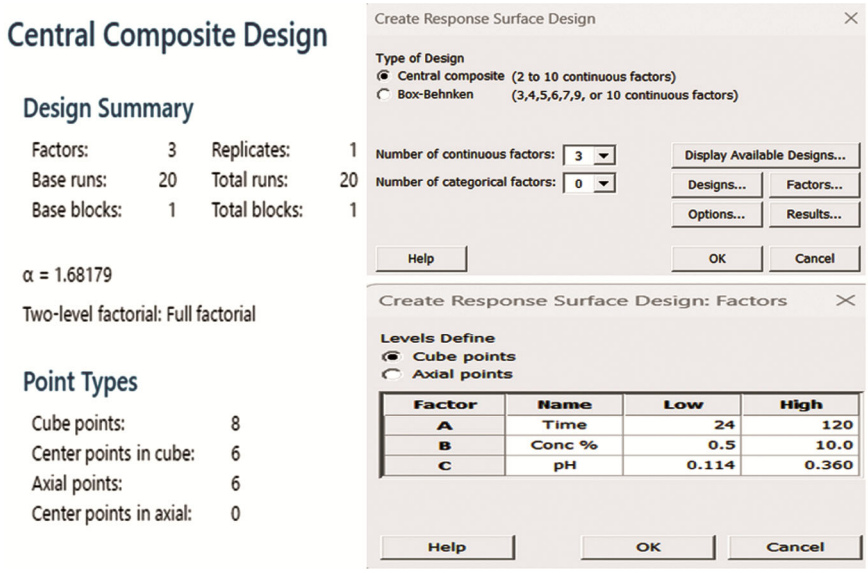

Fig. 1 — DOE Model with CCD

File Edit Data Calc Stat Graph Editor Tools Window Help Assistant

	C1	C2	C3	C4	C5	C6	C7
	StdOrder	RunOrder	PtType	Blocks	Time	Conc %	pH
1	3	1	1	1	24.000	10.0000	0.114000
2	14	2	-1	1	72.000	5.2500	0.443861
3	19	3	0	1	72.000	5.2500	0.237000
4	7	4	1	1	24.000	10.0000	0.360000
5	2	5	1	1	120.000	0.5000	0.114000
6	18	6	0	1	72.000	5.2500	0.237000
7	6	7	1	1	120.000	0.5000	0.360000
8	12	8	-1	1	72.000	13.2385	0.237000
9	5	9	1	1	24.000	0.5000	0.360000
10	11	10	-1	1	72.000	-2.7385	0.237000
11	16	11	0	1	72.000	5.2500	0.237000
12	20	12	0	1	72.000	5.2500	0.237000
13	10	13	-1	1	152.726	5.2500	0.237000
14	13	14	-1	1	72.000	5.2500	0.030139
15	1	15	1	1	24.000	0.5000	0.114000
16	17	16	0	1	72.000	5.2500	0.237000
17	8	17	1	1	120.000	10.0000	0.360000
18	4	18	1	1	120.000	10.0000	0.114000
19	15	19	0	1	72.000	5.2500	0.237000
20	9	20	-1	1	-8.726	5.2500	0.237000

Fig. 2 — Randomized Model by Minitab Software

copper-lean phase is rich in iron and chromium, while the copper-rich matrix lacks iron and chromium. A positive enthalpy of mixing between Cu-Fe and Cu-Cr pairings, which promotes segregation and the formation of both copper-rich and copper-lean phases, is responsible for this discovery. Table 3 and Fig. 4 provide the chemical composition of these phases. Liquid phase separation (LPS) elucidates the uneven distribution of Cr and Fe in the cast sample. As the primary dendritic phase (DR) grows, inter-dendritic (ID) regions develop[1]. Within the $Al_{2.2}CrCuFeNi_2$ alloy, ID liquid undergoes constitutional LPS, dividing into two liquids: Liquid1, rich in Cr and Fe, and $Liquid_2$, rich in Cu. Additionally, slow diffusion in alloys with multiple components may contribute to this phenomenon.

3.2 Corrosion and inhibition of $Cu_{45}Mn_{25}Al_{15}Fe_5Cr_5Ni_5$ HEA

3.2.1 Effect of different concentrations of HNO_3

Figure 5 and Table 4 depict the impact of immersion time on $Cu_{45}Mn_{25}Al_{15}Fe_5Cr_5Ni_5$ HEA subjected to varied concentrations of HNO_3 acid for 120 h. The weight loss per area of $Cu_{45}Mn_{25}Al_{15}Fe_5Cr_5Ni_5$ HEAs increases with higher acid concentrations, as evidenced by the increasing WL values in all cases. Table 5 and Fig. 6 display the CR values of $Cu_{45}Mn_{25}Al_{15}Fe_5Cr_5Ni_5$ HEAs immersed in various amounts of HNO_3 acid for 120 h. Their chemical composition and the stability of their oxide layer influence their corrosion behavior under the tested conditions[1]. Fig. 7 provides visual representations of HEAs tested in different concentrations of HNO_3 acid after 120 h of immersion. As the concentrations of nitric acid increase, the CR increases, as shown in Table 4 and Fig. 7.

3.2.2. Effect of different inhibitors

The measurements of weight loss at 293 K after 120 h of immersion to evaluate the impact of introducing nanoparticles as corrosion inhibitors on $Cu_{45}Mn_{25}Al_{15}Fe_5Cr_5Ni_5$ HEAs in 0.5% HNO_3 solution. Fig. 8 illustrates the relationship between inhibitor concentration and CR for $Cu_{45}Mn_{25}Al_{15}Fe_5Cr_5Ni_5$ HEA in 0.5% HNO_3 solutions. The findings show a reduction in the weight loss of $Cu_{45}Mn_{25}Al_{15}Fe_5Cr_5Ni_5$ HEA in the inhibitor solution compared to the blank 0.5% HNO3 solution. The inhibitors impeded the

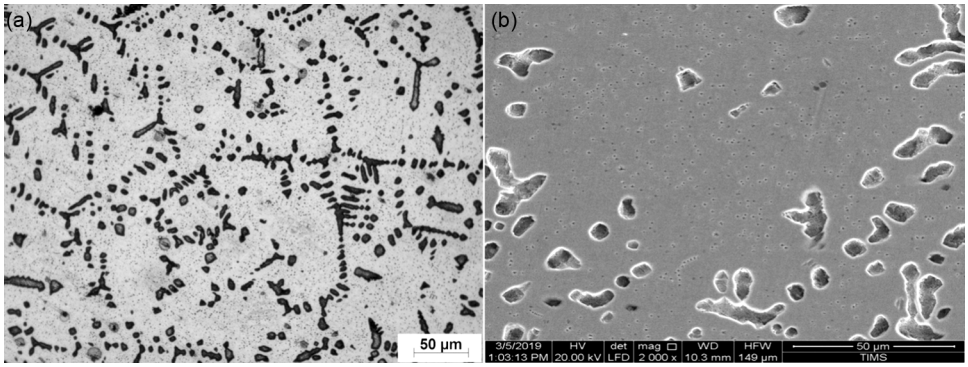

Fig. 3 — Cast $Cu_{45}Mn_{25}Al_{15}Fe_5Cr_5Ni_5$ HEA (a) optical micrograph, and (b) SEM micrograph

Table 3 — The EDX analysis of cast $Cu_{45}Mn_{25}Al_{15}Fe_5Cr_5Ni_5$ HEA

Spots No.	Elements, at. %					
	Cu	Mn	Al	Ni	Fe	Cr
Spot 1	49.84	26.84	14.51	7.19	1.26	0.36
Spot 2	27.13	22.41	23.38	12.24	7.43	7.40

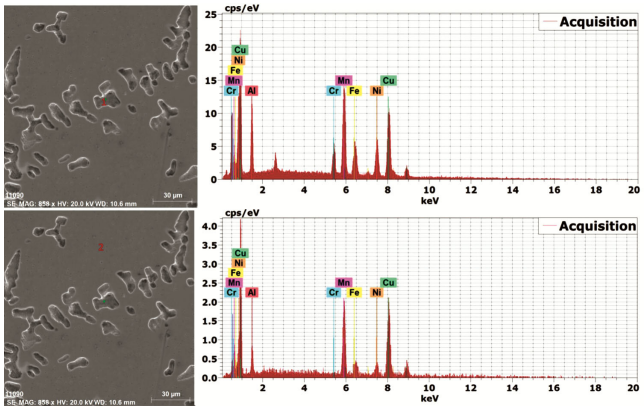

Fig. 4 — The EDX analysis of cast $Cu_{45}Mn_{25}Al_{15}Fe_5Cr_5Ni_5$ HEA, spot (1) copper lean & spot and (2) copper-rich phases

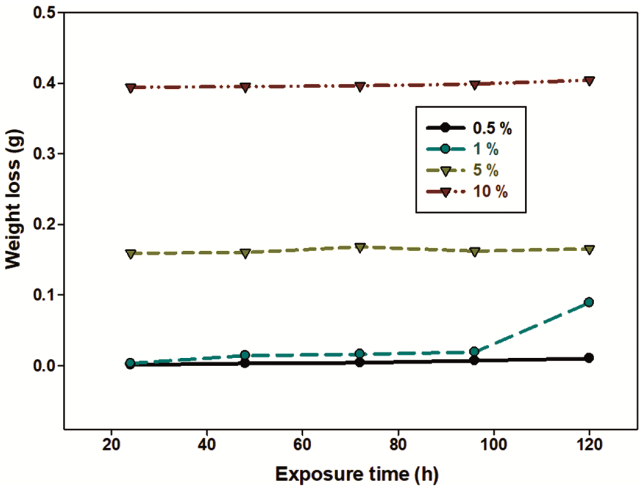

Fig. 5 — The WL-Time plots for $Cu_{45}Mn_{25}Al_{15}Fe_5Cr_5Ni_5$ HEA over 120 h in varying concentrations of HNO_3 solution

corrosion process when they adsorbed onto the surface of the $Cu_{45}Mn_{25}Al_{15}Fe_5Cr_5Ni_5$ HEA[26,27]. This information shows that Nano-TiO_2, Nano-SiO_2, and Nano-ZnO can stop $Cu_{45}Mn_{25}Al_{15}Fe_5Cr_5Ni_5$ HEA from dissolving in a 0.5% HNO_3 solution. Based on the weight loss data over 120 h, Table 6 displays the corrosion rate, surface coverage, and inhibition efficiency. The results show that adding Nano TiO_2, Nano-SiO_2, and Nano-ZnO significantly reduces the corrosion of $Cu_{45}Mn_{25}Al_{15}Fe_5Cr_5Ni_5$ HEA in 0.5% HNO_3. The addition of Nano-TiO_2 raises the inhibition efficiency (%) to 89.8%. The formation of a thin, stable passive coating on the metal surface is believed to be responsible for the significantly lower corrosion rates observed when inhibitors are present compared to the free solution[28].

3.3 Surface Morphology

Figure 9 provides SEM micrographs and spot EDX results of the corroded $Cu_{45}Mn_{25}Al_{15}Fe_5Cr_5Ni_5$ HEAs in 5% and 10% HNO_3 solutions. Table 7 presents the spot EDX results of the corroded $Cu_{45}Mn_{25}Al_{15}Fe_5Cr_5Ni_5$ HEAs. Figs. 9(a & b) show the elemental distribution of the corroded $Cu_{45}Mn_{25}Al_{15}Fe_5Cr_5Ni_5$ HEA in 5% HNO_3 solutions, while Figs. 9(c & d) depict it in 10% HNO_3 solutions. Additionally, Fig. 10 illustrates the elemental distribution of the corroded $Cu_{45}Mn_{25}Al_{15}Fe_5Cr_5Ni_5$ HEAs in a 5% HNO_3 solution, while Fig. 11 shows it in a 10% HNO_3 solution. The figures show the extent of localized corrosion and general corrosion, which increase as HNO_3 concentrations rise. The EDX results of the corroded $Cu_{45}Mn_{25}Al_{15}Fe_5Cr_5Ni_5$ HEAs in the presence of different inhibitors are shown in Table 8 and Fig. 12. The lowest oxygen content observed in TiO_2 aligns with the CR values obtained

in Table 6. The elemental distributions are shown in Figs. 13-15 when nano-TiO_2, nano-SiO_2, and nano-ZnO inhibitors are present. These mappings also confirm that Nano-TiO_2 exhibits the best distribution of elements within the protective layers, which is responsible for lowering the CR values. Localized corrosion decreases when inhibition is used, particularly with TiO_2. The presence of protective layers, which prevent further corrosion, could be the reason for this. In the SEM and mapping images, the dendritic phase (rich in Cr and Fe) exhibits high corrosion resistance in nitric acid concentrations. The presence of chromium oxide on the HEA's surface, which aids in reducing the CR, may be responsible for this increased resistance. Adding inhibitors to the nitric acid led to the formation of additional oxides on the surface, which act as barriers to protect the HEA from corrosion.

Table 4 — The WL findingsfor $Cu_{45}Mn_{25}Al_{15}Fe_5Cr_5Ni_5$ HEA immersed in different quantities of HNO_3 acid after 120 h

HNO_3Conc.	Time, h				
%	24	48	72	96	120
0.5	0.001	0.003	0.004	0.007	0.010
1	0.003	0.014	0.016	0.019	0.089
5	0.159	0.16	0.168	0.162	0.165
10	0.394	0.395	0.396	0.3987	0.404

Table 5 — The WL and CR valuesfor $Cu_{45}Mn_{25}Al_{15}Fe_5Cr_5Ni_5$ HEA were immersed in varying amounts of HNO_3 acid for 120 h

HNO_3Conc., %	WL, g	CR, mm/y
0.5	0.010	1.045
1	0.089	9.299
5	0.165	17.240
10	0.404	42.213

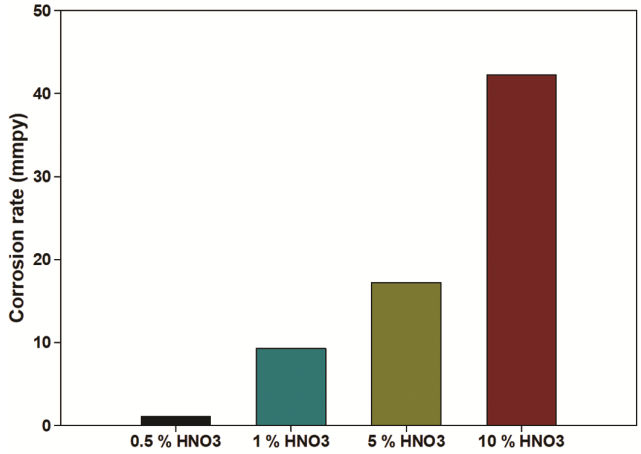

Fig. 6 — The variation of CR for $Cu_{45}Mn_{25}Al_{15}Fe_5Cr_5Ni_5$ HEA immersed in solutions of varying concentrations of HNO_3

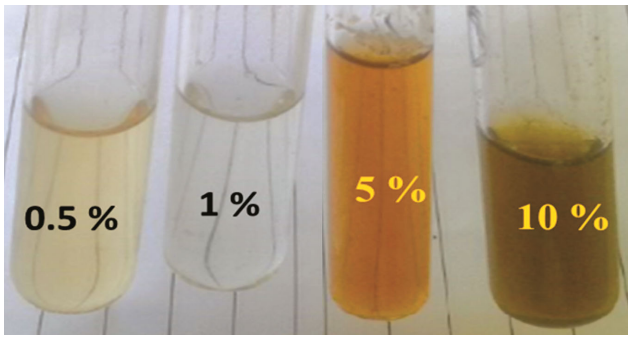

Fig. 7 — Images of HEAs in varying quantities of HNO_3 acid following 120 h of immersion testing

3.4 Statistical Analysis of Corrosion Feature of HEA

3.4.1 Analysis of Variance (ANOVA)

The F-test and p-value confirmed the statistical significance of the regression model. Table 9 presents the ANOVA results of the response surface model. In statistical analysis, the significance of a coefficient is typically assessed by its p-value; lower p-values

Table 6 — The CR, the θ, and the IE% of $Cu_{45}Mn_{25}Al_{15}Fe_5Cr_5Ni_5$ HEA in 0.5 % HNO_3 solution in the absence/presence of different inhibitors obtained by the WL method at 20°C

Conditions	CR, mm/y	θ	IE, %
Blank (0.5 % HNO_3)	1.045	--	--
TiO_2	0.107	0.898	89.8
SiO_2	0.129	0.877	87.7
ZnO	0.230	0.779	77.9

Table 7 — The EDX findings of corroded $Cu_{45}Mn_{25}Al_{15}Fe_5Cr_5Ni_5$ HEA in varying concentrations of HNO_3solution

Spots No.	Elements, at. %							
	N	O	Cu	Mn	Al	Ni	Fe	Cr
Spot 3	10.1	16.5	69.3	0.0	1.4	0.7	1.5	0.5
Spot 4	5.0	22.6	33.4	11.2	5.5	0.5	11.6	10.3
Spot 5	7.3	4.7	3.4	23.4	6.3	0.4	27.2	27.3

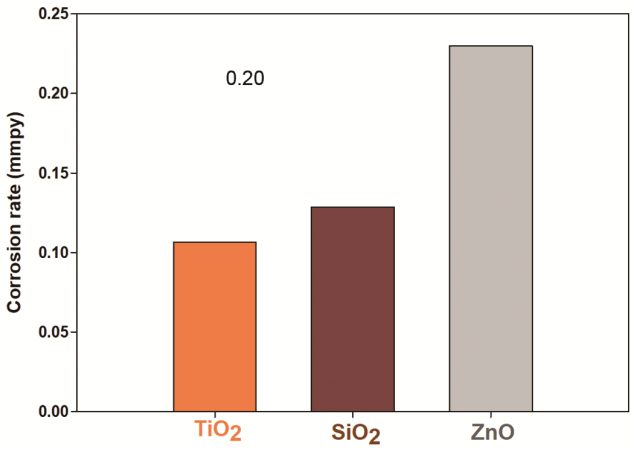

Fig. 8 — The variation of CR for $Cu_{45}Mn_{25}Al_{15}Fe_5Cr_5Ni_5$ HEA in 0.5 % HNO_3 solution in the absence/presence of different inhibitors obtained by the WL method at 20 °C

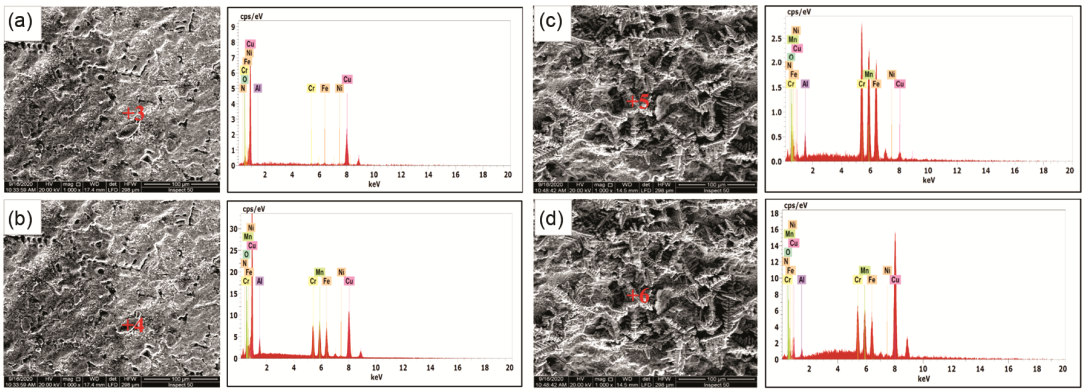

Fig. 9 — The SEM morphologies and EDX results of cast $Cu_{45}Mn_{25}Al_{15}Fe_5Cr_5Ni_5$ HEA in HNO_3 solutions of concentration (a and b) 5% and (c and d) 10%

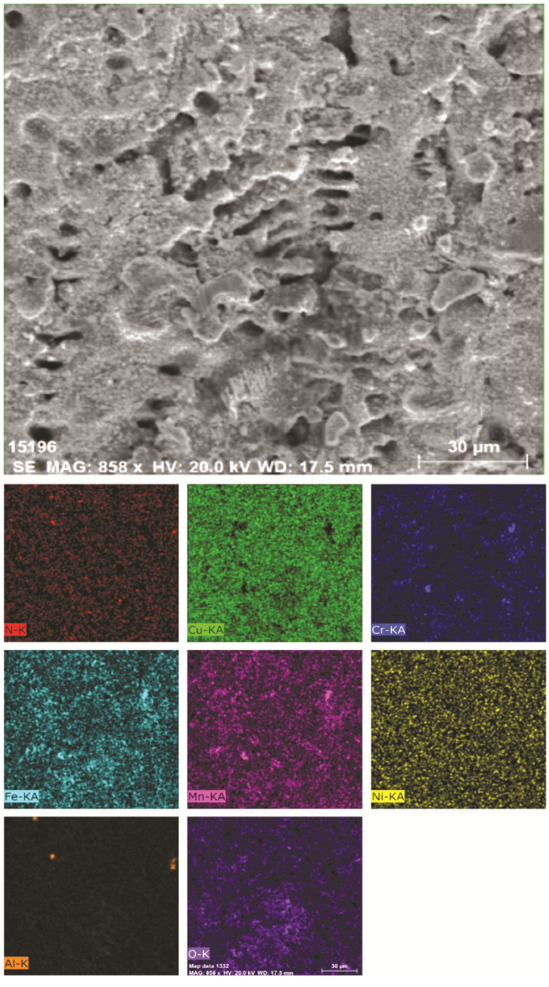

Fig. 10 — Mapping of the corroded $Cu_{45}Mn_{25}Al_{15}Fe_5Cr_5Ni_5$ HEA in 5% HNO_3 solution

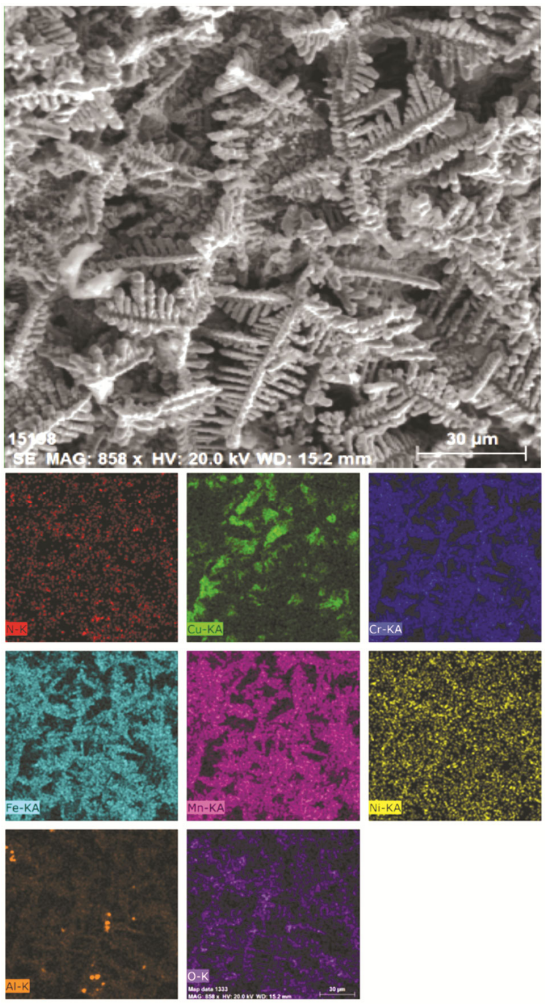

Fig. 11 — Mapping of the corroded $Cu_{45}Mn_{25}Al_{15}Fe_5Cr_5Ni_5$ HEA in 10% HNO_3 solution

indicate greater significance. A p-value below 0.05 is commonly considered statistically significant for model terms[29]. In Table 9, the presence of a single asterisk marking the regression model's p-value suggests the significance of the model terms, indicating the least significant level. Furthermore, the p-values for the linear and interaction coefficients are also below 0.05, indicating their statistical significance. A higher R^2 value suggests that the

Table 8 — The EDX results of corroded $Cu_{45}Mn_{25}Al_{15}Fe_5Cr_5Ni_5$ HEA in 10% HNO_3 solution and different inhibitors

Spots No.	Elements, at. %										
	N	O	Cu	Mn	Al	Ni	Fe	Cr	Ti	Si	Zn
Spot 7	0.0	8.0	11.8	20.1	7.0	1.7	25.8	23.8	1.7	0.0	0.0
Spot 8	1.8	12.8	10.55	18.8	9.4	0.9	22.4	23.2	0.0	0.2	0.0
Spot 9	3.3	53.2	25.0	1.9	13.2	0.5	1.2	0.9	0.0	0.0	0.7

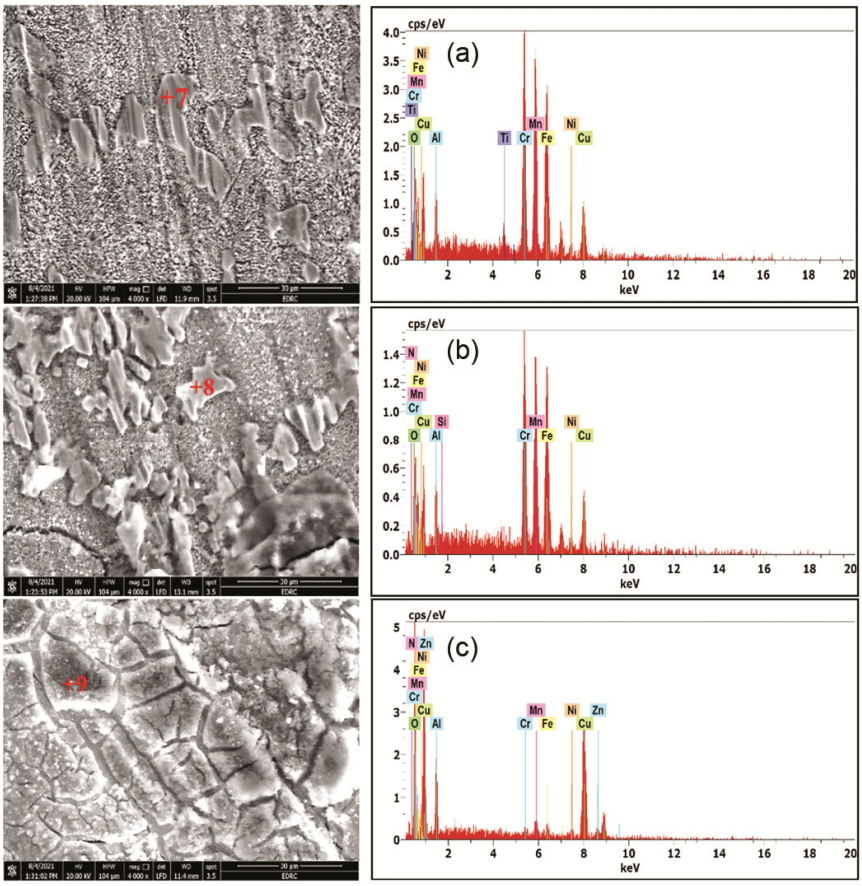

Fig. 12 — The SEM morphologies and EDX results of cast $Cu_{45}Mn_{25}Al_{15}Fe_5Cr_5Ni_5$ HEA in 10%HNO_3 solution and inhibitor (a) TiO_2, (b) SiO_2, and (c) ZnO

predicted values closely match the experimental data. The model appears to be accurate, as the adjusted R^2 value of 99.51% closely aligns with the expected R^2 value of 98.63%.

3.4.2 Surface and Contour Plots

Response surface plots, both two- and three-dimensional, are valuable tools for identifying the appropriate response values and operating conditions. A contour plot, a two-dimensional representation of the response surface, employs contour lines of constant responses to connect regions with similar responses. However, for a clearer depiction of the response, a surface plot in three dimensions is preferable[30]. The 3D response surface plot for time, HNO_3 concentration, and pH in Fig. 16 illustrates how interaction effects influence the corrosion of $Cu_{45}Mn_{25}Al_{15}Fe_5Cr_5Ni_5$ HEA. It confirms that the WL increases somewhat with longer immersion durations. Considering process lead time, an ideal duration of less than 120 hours may be preferable to meet productivity and production output targets. Additionally, the CR is observed to be directly proportional to the concentration of HNO_3. As shown in Fig. 16, the WL attains its peak efficiency when both time and HNO_3 concentration are minimized.

3.4.3 Main Effects

Figure 17 illustrates the major effect plots, also known as factorial plots, where each investigated

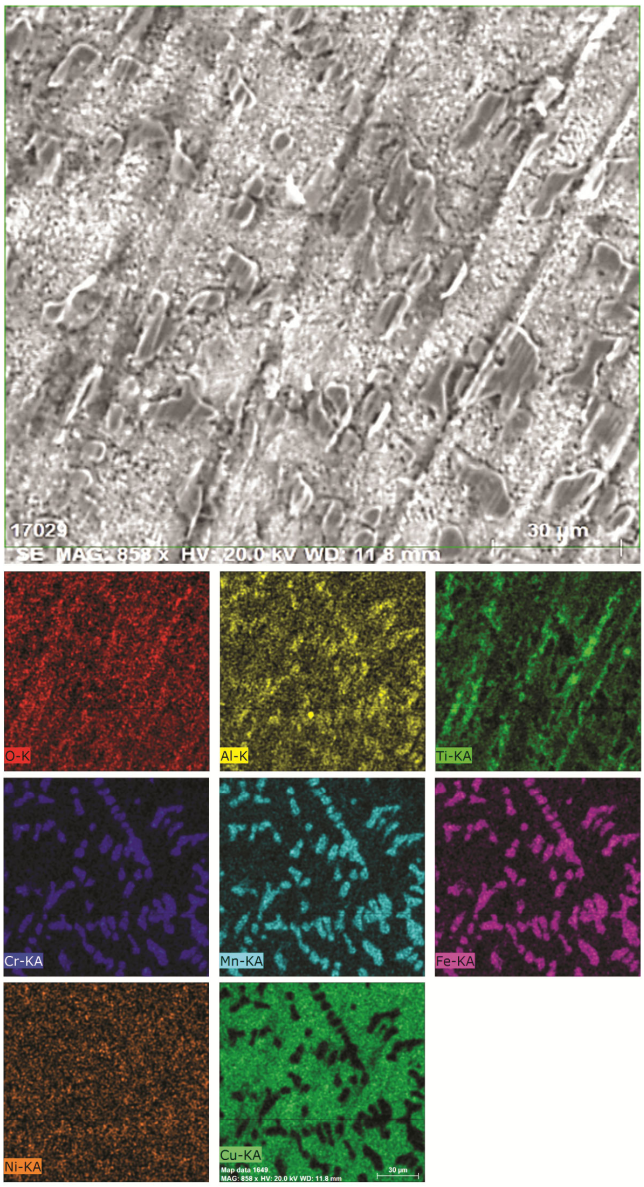

Fig.13 — Mapping of the corroded $Cu_{45}Mn_{25}Al_{15}Fe_5Cr_5Ni_5$ HEA in 10% HNO_3 solution and TiO_2 inhibitor

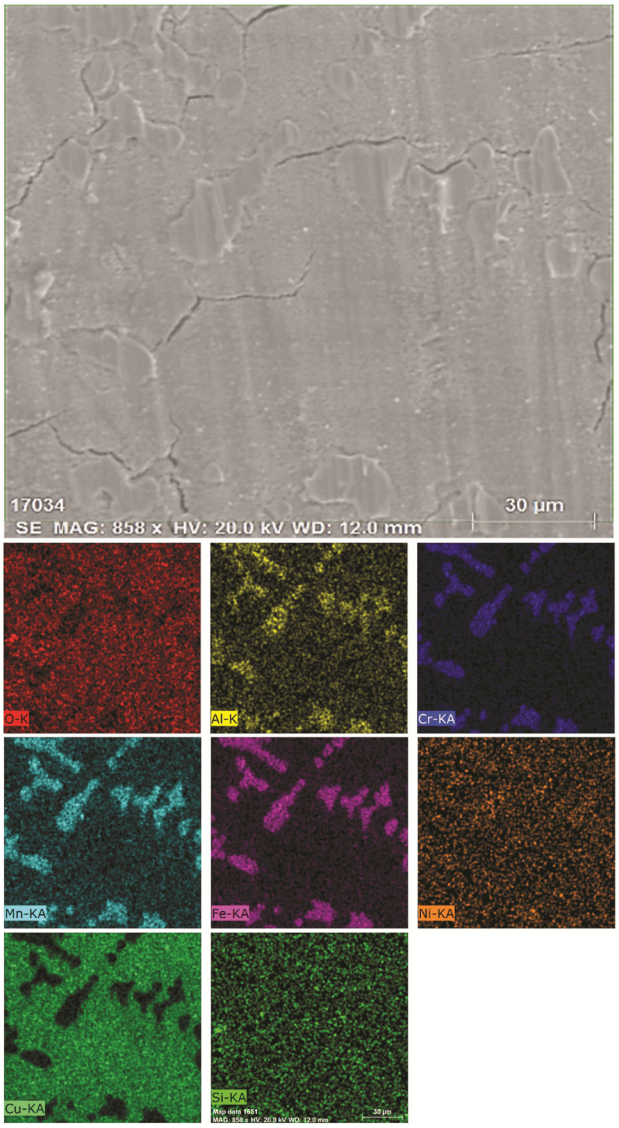

Fig. 14 — Mapping of the corroded $Cu_{45}Mn_{25}Al_{15}Fe_5Cr_5Ni_5$ HEA in 10% HNO_3 solution and SiO_2 inhibitor

parameter demonstrates its effect. It's important to note that the values displayed at each point represent the average WL at that level, relative to all other parameter levels, with the overall mean plotted across all panels. Fig. 18 displays the Pareto chart of the standardized effect for the CR, both with a confidence level of 95%. The estimated regression coefficients in the model (Eqs4 and 5) for weight loss and corrosion rate reveal the main effects of time, pH, and concentration percentage (Conc.%) on cast $Cu_{45}Mn_{25}Al_{15}Fe_5Cr_5Ni_5$ HEA. The p-values for these main effects are below the accepted threshold of 0.05, indicating statistical significance. Additionally, the p-value for 2-way interactions is 0.011. The most significant effects are attributed to time, pH, and concentration percentage, while the effects of other coefficients were found to be insignificant.

The weight loss (WL) regression models exhibit an R-squared (R^2) value of 99.69% and an adjusted R-squared (adj R^2) value of 98.63%. Similarly, in a comparable regression model for the cast HEA's corrosion rate (CR), R^2 = 95.05% and modified R^2 = 92.16%. Mathematical models (Eqs4 and 5) were developed to understand the impact of various variables and their interactions on weight loss and corrosion rate. As the HNO_3 concentration increases, the medium becomes more aggressive, leading to a

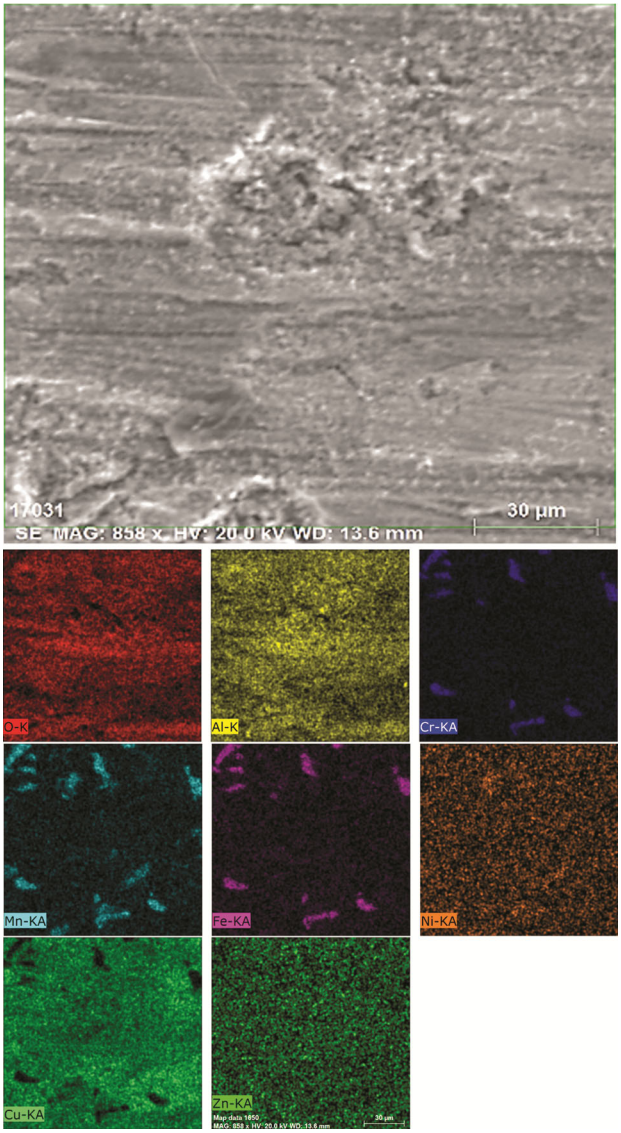

Fig. 15 — Mapping of the corroded $Cu_{45}Mn_{25}Al_{15}Fe_5Cr_5Ni_5$ HEA in 10% HNO_3 solution and ZnO inhibitor

natural increase in weight loss. This increase in WL corresponds to a higher corrosion rate for the cast $Cu_{45}Mn_{25}Al_{15}Fe_5Cr_5Ni_5$ HEA. The highest CR of 42.2128 mm/y was observed at a 10% HNO_3 concentration, while the lowest was observed at a 0.5% HNO_3 concentration.

Mathematical modelsfor WL (g) =-0.0564 + 0.000479 Time (h) + 0.03037 Conc % + 0.1607 pH+ 0.000004 Time (h)*Time (h) + 0.001115 Conc %*Conc % - 0.000012 Time (h)*Conc % - 0.002801 Time (h)*pH …(4)

Mathematical models forCR (mm/Y) = 16.9 - 1.078 Time (h) + 18.95 Conc % + 18.8 pH + 0.00906 Time (h)*Time (h) + 0.303 Conc %*Conc % - 0.1704 Time (h)*Conc % - 0.23 Time (h)*pH …(5)

3.4.4 Residuals plots

A normal probability plot in Fig. 19 illustrates the normal probability distribution of WL for cast Cu45Mn25Al15Fe5Cr5Ni5 HEA. The residuals form a straight line in the plot, suggesting that the errors follow a normal distribution[31]. Furthermore, the residuals exhibit an even distribution along the mean line, and the absence of any noticeable outliers confirms the normality of the distribution. Moreover, there is no discernible trend in the residual plot for the weight loss of cast $Cu_{45}Mn_{25}Al_{15}Fe_5Cr_5Ni_5$ HEA, further confirming the data's normality.

3.4.5 Interaction Plot

An interaction plot is a valuable tool for illustrating how two categorical factors relate to a continuous response[32]. These plots reveal the combined effect of two or more experimental parameters on the response

Table 9 — ANOVA results for WL of casted $Cu_{45}Mn_{25}Al_{15}Fe_5Cr_5Ni_5$ HEA

Source	DF	Adj SS	Adj MS	F-Value	p-Value
Model	7	0.489849	0.069978	546.72	0.0001
Linear	3	0.487446	0.162482	1269.43	0.0001
Time (h)	1	0.001679	0.001679	13.11	0.004
Conc %	1	0.431713	0.431713	3372.86	0.000
pH	1	0.000191	0.000191	1.49	0.246
Square	2	0.001920	0.000960	7.50	0.008
Time (h)*Time (h)	1	0.000271	0.000271	2.12	0.171
Conc %*Conc %	1	0.001649	0.001649	12.88	0.004
2-Way Interaction	2	0.001728	0.000864	6.75	0.011
Time (h)*Conc %	1	0.000046	0.000046	0.36	0.559
Time (h)*pH	1	0.001330	0.001330	10.39	0.007
Error	12	0.001536	0.000128		
Total	19	0.491385			

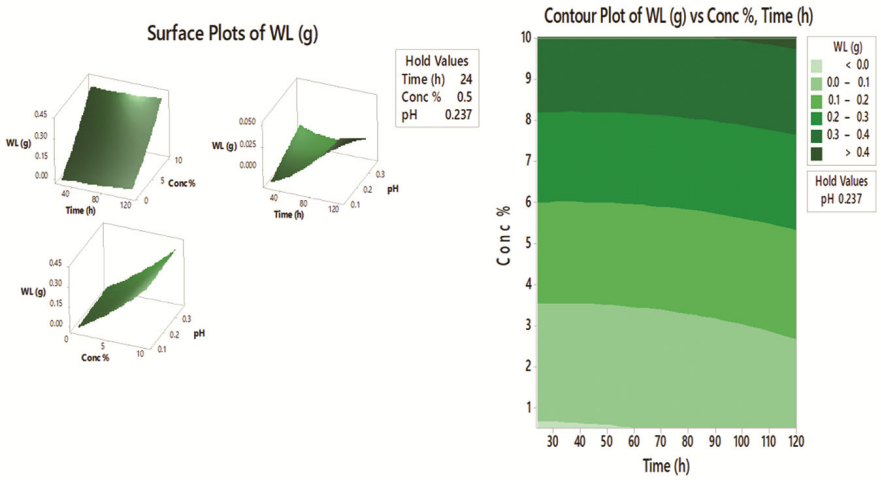

Fig. 16 — Effects of time, concentration HNO_3, and pH on corrosion of $Cu_{45}Mn_{25}Al_{15}Fe_5Cr_5Ni_5$ HEA

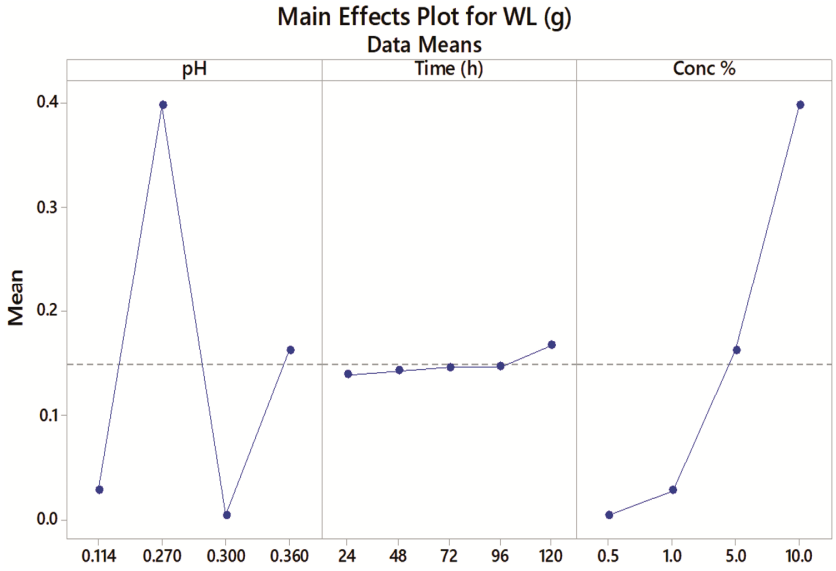

Fig. 17 — Plots depicting the main effect of the variables on WL

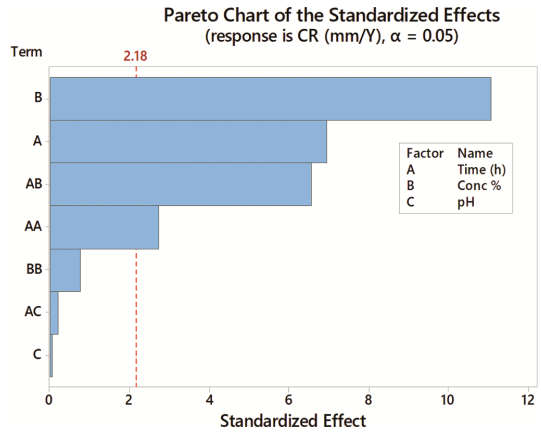

Fig. 18 — Pareto chart of the standardized effect for CR of $Cu_{45}Mn_{25}Al_{15}Fe_5Cr_5Ni_5$ HEA

(in this case, weight loss, WL), unlike main effect plots, which show the effect of each parameter on the response individually. Fig. 20 displays the corrosion behavior of $Cu_{45}Mn_{25}Al_{15}Fe_5Cr_5Ni_5$ HEA under different combinations of factors. Three variables interact to generate a total of six interaction plots. Each plot illustrates various interactions, and their slope and the distance between minimum and maximum values can be analyzed. The absence of horizontal slopes in Fig. 20's lines indicates strong interactions between the depicted characteristics. The response mean of $Cu_{45}Mn_{25}Al_{15}Fe_5Cr_5Ni_5$ HEA in HNO_3 media varies from low to high levels of the input variable, depending on the level of the second experimental variable. Table 9 further

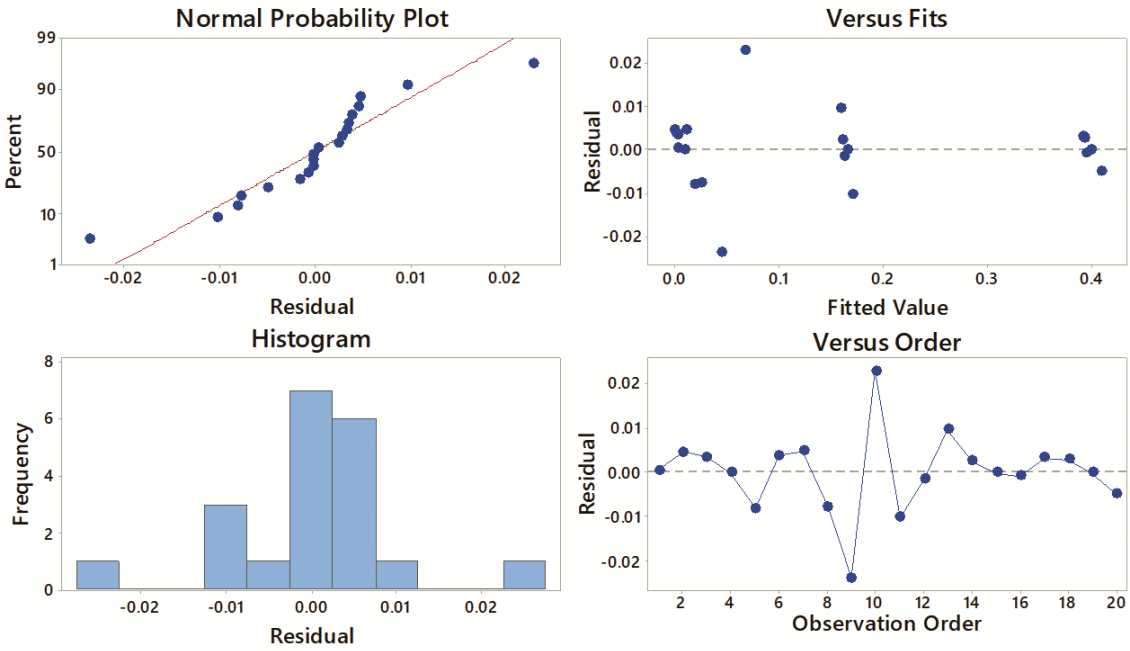

Fig. 19 — Residuals plots for WL

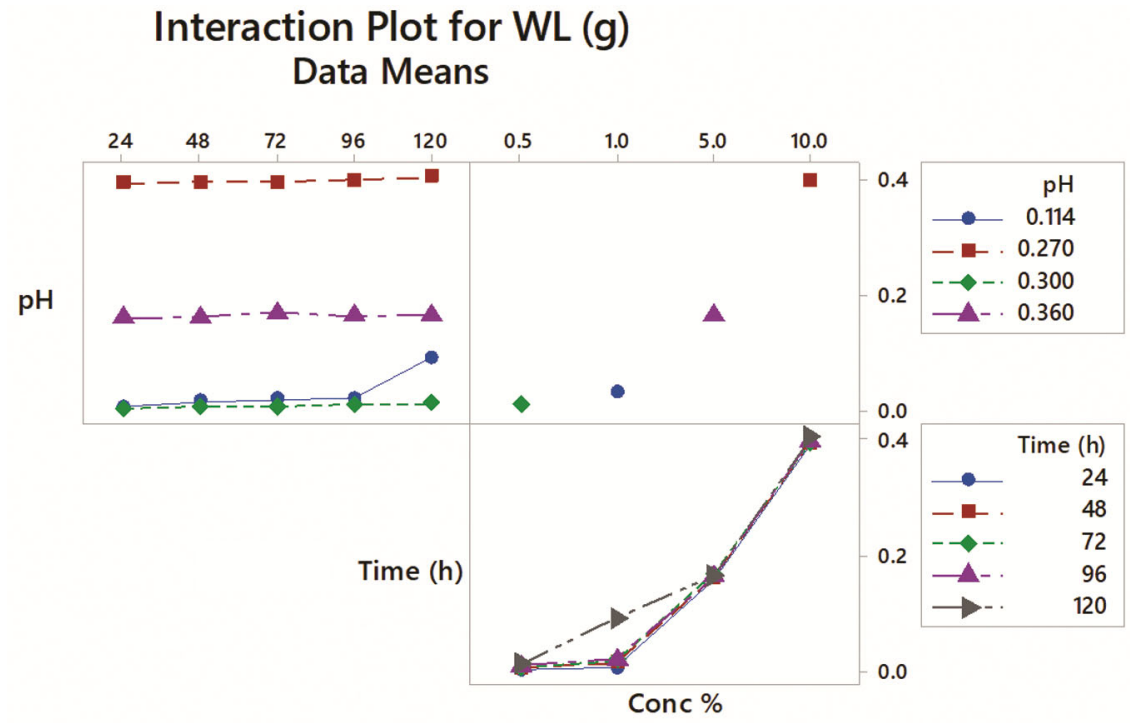

Fig. 20 — Interaction effects between the corrosion cast $Cu_{45}Mn_{25}Al_{15}Fe_5Cr_5Ni_5$ HEA

confirms the significance of the interaction between time and pH, indicating that the combination of time significantly influences the corrosion rate of $Cu_{45}Mn_{25}Al_{15}Fe_5Cr_5Ni_5$ HEA. Additionally, Table 10 provides details on response optimization for WL and CR. At a pH of 0.248, a concentration of 5% HNO_3, and a duration of 24 h, the MINITAB optimizer identified an optimal fit of 81.64%.

Table 10 — Response Optimization (WL (g), CR (mm/y))

Parameters						
Response	Goal	Lower	Target	Upper	Weight	Importance
WL (g)	Target	0.0010	0.159	0.404	1	1
CR (mm/Y)	Target	0.5224	83.067	205.839	1	1
Solution						
Solution	Time (h)	Conc %	pH	WL (g) Fit	CR (mm/Y) Fit	Composite Desiability
1	25	5.01010	0.248182	0.159168	81.6494	0.991037

Multiple Response Prediction

Variable	Setting
Time (h)	24
Conc %	5.0101
pH	0.248182

Response	Fit	SE Fit	95% CI	95% PI
WL (g)	0.15917	0.00757	(0.14267, 0.17566)	(0.12951, 0.18883)
CR (mm/Y)	81.65	9.51	(60.94, 102.36)	(44.40, 118.90)

4 Conclusion

The research has led to a thorough analysis of experimental data, presenting a novel methodology for identifying optimal corrosion parameters that offer both effectiveness and robustness. The corrosion behavior of cast Cu45Mn25Al15Fe5Cr5Ni5 HEA was carefully assessed in HNO_3 solutions of varying concentrations (0.5%, 1%, 5%, and 10%). The SEM and EDX analyses of the cast HEA identified inter-dendritic (ID) regions and the primary dendritic phase (DR). A mathematical model was developed to link the alloy's properties with processing parameters, aiming to clarify their impact on corrosion behavior. As HNO_3 concentration increased with the addition of inhibitors such as Nano-TiO_2, Nano-SiO_2, or Nano-ZnO reduced CR values from 1.04 mm/y to 0.11, 0.12, or 0.22 mm/y, respectively, in 0.5% HNO_3. SEM, spot EDX, and elemental mapping of corroded surfaces in 5% and 10% HNO_3 solutions revealed that Nano-TiO_2 provided the lowest corrosion rates, minimal localized corrosion, and formed protective layers.

Conflicts of interest

The authors declare that they have no conflicts of interest.

Data Availability

The data that support the findings of this study are available upon reasonable request from the authors.

References

1 Kellenberger A, Duca D A, Dan M L & Medeleanu M, *Materials*, 15 (2022) 2918.
2 Khalifa O R M, Kassab A K, Mohamed H A & Ahmed S Y, *J Am Sci*, 6 (2010) 487.
3 Kania H, *Coatings*, 13 (2023) 216.
4 Antonijevic M M & Petrovic M B, *Int J Electrochem Sci*, 3 (2008) 1.
5 Abdelghafar K A, Ibrahim M M, Shoeib M A & Waly M A, Mater Res Express, 7 (2020) 016579.
6 Bamisaye O S, Maledi N, Merwe J V & Bodunrin M O, *Int J Refract Metal Hard Mater*, 121 (2024) 106661.
7 Abolkassem S A, El-Hadad S & Mohamed L Z, *Arab J Sci Eng*, (2024).
8 Nartita R, Ionita D & Demetrescu I, *Crystals*, 14 (2024) 451.
9 Aly H A, Abdelghafar K A, Gaber G A & Mohamed L Z, *J Mater Eng Perform*, 30 (2021) 1430.
10 Mohamed L Z, Abdelghafar K A, Aly H A & Gaber G A, *Int J Metalcast*, 17 (2023) 1791.
11 Vahdani M, Ghazavi M & Roustaei M, *Int J Eng (IJE), Trans A: Basics*, 33 (2020) 1826.
12 Anderson-Cook C M, Borror C M & Montgomery D C, *J Statist Planning Infer*, 139 (2009) 629.
13 Doniavi A, Hosseini A & Ranjbary G, *Int J Eng, Trans C: Asp*, 29 (2016) 1307.
14 Al-Amiery A A, Isahak W N R W & Al-Azzawi W K, *Lubricants*, 11 (2023) 174.
15 Morais W R S, Silva J S, Queiroz N M P, Zanta C L P S, Ribeiro A S & Tonholo J, *Appl Sci*, 13 (2023) 7482.
16 Chobba M B, Weththimuni M L, Messaoud M, Urzi C & Licchelli M, *Coatings*, 14 (2024) 203.
17 Aminuzzaman M, Ying L P, Goh W-S & Watanabe A, *Bull Mater Sci*, 41 (2018) 50.
18 Raha S & Ahmaruzzaman M, *Nanoscale Adv*, 4 (2022) 1868.
19 Shozib I A, Ahmad A, Abdul-Rani A M, Beheshti M & Aliyu A A, *Corros Rev*, 40 (2022) 1.
20 Gaber G A, Mohamed L Z & Abd-Elaziem W, *Egypt J Chem*, (2024).
21 Gaber G A, Abdelfatah A & Mohamed L Z, *Egypt J Chem*, 67 (2024) 201.
22 Gaber G A, Mohamed L Z, Elkady OA, Elsayed A he & Abolkkassem SA, *India J Pure Appl Phys,* 62 (2014)743.
23 Gaber G A, Mohamed L Z & Hamdy G, *Egypt J Chem*, (2024).

24 Dean A, Morris M, Stufken J & Bingham D, Handbook of design and analysis of experiments, CRC Press, (2015).
25 Hashem S A M, Gaber G A, Hussein W A & Ahmed A S I, *Res Mater*, 23 (2024) 100606.
26 Yin C, Kong M, Zhang J, Wang Y, Ma Q, Chen Q & Liu H, *ACS Omega*, 5 (2020) 2620.
27 Zunita M & Rahmi V A, *Chem Africa*, 7 (2024) 505.
28 Harvey T, Walsh F C & Nahlé A, *J Mol Liq*, 266 (2018).
29 Tansuğ G, Tüken T, Kıcır N & Erbil M, *Ionics*, 20 (2014) 287.
30 Anadebe V C, Onukwuli O D, Omotioma M & Okafor N A, *S Afr J Chem*, 71 (2018) 51.
31 Salam K K, Agarry S E, Arinkoola A O & Shoremekun I O, *Biotechnol J Int*, 7 (2015) 68.
32 Soltani N, Behpour M, Ghoreishi S M & Naeimi H, *Corros Sci*, 52 (2010)1351.